

A DEDICATED CHANDRA ACIS OBSERVATION OF THE CENTRAL COMPACT OBJECT IN THE CASSIOPEIA A SUPERNOVA REMNANT

G. G. PAVLOV

Pennsylvania State University, 525 Davey Laboratory, University Park, PA 16802, USA; pavlov@astro.psu.edu

AND

G. J. M. LUNA

Smithsonian Astrophysical Observatory, 60 Garden Street, Cambridge, MA 02138, USA; gluna@cfa.harvard.edu

To be published in ApJ 2009 October, vol. 702

ABSTRACT

We present results of a recent *Chandra* X-ray Observatory observation of the central compact object (CCO) in the supernova remnant Cassiopeia A. This observation was carried out in an instrumental configuration that combines a high spatial resolution with a minimum spectral distortion, and it allowed us to search for pulsations with periods longer than ≈ 0.68 s. We found no evidence of extended emission associated with the CCO, nor statistically significant pulsations (the 3σ upper limit on pulsed fraction is about 16%). The fits of the CCO spectrum with the power-law model yield a large photon index, $\Gamma \approx 5$, and a hydrogen column density larger than that obtained from the SNR spectra. The fits with the blackbody model are statistically unacceptable. Better fits are provided by hydrogen or helium neutron star atmosphere models, with the best-fit effective temperature $kT_{\text{eff}}^{\infty} \approx 0.2$ keV, but they require a small star's radius, $R = 4\text{--}5.5$ km, and a low mass, $M \lesssim 0.8M_{\odot}$. A neutron star cannot have so small radius and mass, but the observed emission might emerge from an atmosphere of a strange quark star. More likely, the CCO could be a neutron star with a nonuniform surface temperature and a low surface magnetic field (the so-called anti-magnetar), similar to three other CCOs for which upper limits on period derivative have been established. The bolometric luminosity, $L_{\text{bol}}^{\infty} \sim 6 \times 10^{33}$ erg s⁻¹, estimated from the fits with the hydrogen atmosphere models, is consistent with the standard neutron star cooling for the CCO age of 330 yr. The origin of the surface temperature nonuniformity remains to be understood; it might be caused by anisotropic heat conduction in the neutron star crust with very strong toroidal magnetic fields.

Subject headings: stars: neutron — supernovae: individual (Cassiopeia A)

1. INTRODUCTION

Cassiopeia A (Cas A) is the famous remnant of a Type II supernova explosion that was apparently detected about 330 years ago (Aschworth 1980). The compact X-ray source at the center of Cas A was discovered in the first-light *Chandra* observation (Tananbaum 1999) and then found in archival *ROSAT* and *Einstein* images (Aschenbach 1999; Pavlov & Zavlin 1999). It is considered as a prototype of the so-called compact central objects (CCOs) in supernova remnants, which are possibly neutron stars (NSs) with properties very different from those of radio pulsars (Pavlov et al. 2002).

The analysis by Pavlov et al. (2000) and Chakrabarty et al. (2001) of first *Chandra* observations of the Cas A CCO with the ACIS and HRC detectors has shown that it is a pointlike source with a flux $F_X \approx (8\text{--}9) \times 10^{-13}$ ergs s⁻¹ cm⁻² in the 0.6–6 keV band. The source showed no periodicity, with an upper limit on the pulsed fraction of 35% for $P > 20$ ms. Its spectrum was found to be consistent with an absorbed blackbody (BB) model [$N_{\text{H},22} \equiv N_{\text{H}}/10^{22}$ cm⁻² ≈ 0.8 , $kT = 0.5\text{--}0.6$ keV, $R = (0.3\text{--}0.5)D_{3.4}$ km, where $D_{3.4} = D/3.4$ kpc is the distance scaled to the remnant's estimated distance; Reed et al. 1995] or with a steep power-law (PL) model ($N_{\text{H},22} \approx 2$, photon index $\Gamma = 3\text{--}4$).

Based on the X-ray properties of the Cas A CCO, Pavlov et al. and Chakrabarty et al. suggested that its

thermal-like radiation might be interpreted as emitted from hot spots at the NS surface, similar to those seen in some young radio pulsars and accreting X-ray pulsars. However, this source shows no indications of pulsar activity (such as radio or γ -radiation, or a pulsar wind nebula), the emitting region is unusually hot compared to radio pulsars, and the source flux does not show variations expected for an accreting object. Pavlov et al. (2000) and Chakrabarty et al. (2001) speculated that the unusual properties of this source might be caused by an extremely high magnetic field, $B \sim 10^{14}\text{--}10^{15}$ G, similar to those of anomalous X-ray pulsars (AXPs) and soft γ -ray repeaters (SGRs), commonly known as “magnetars”, but they concluded that more observations were required to understand the true nature of this CCO from the spectral and timing analysis.

Since the discovery of the CCO, Cas A has been observed many times with *Chandra*. In addition to about 90 short (1–10 ks) ACIS and HRC calibration observations, two 50 ks ACIS-S3 observations (2000 January and 2002 February), three 50 ks HRC observations (1999 December, 2000 October, and 2001 September), and a 70 ks ACIS/HETG observation (2001 May) have been carried out. Finally, Cas A was observed with ACIS-S3 in 2004 February – May (9 pointings, 40–170 ks exposures) for a total exposure of about 1 Ms. Unfortunately, the vast amount of data collected in those observations has not added much to our understanding of the CCO.

The results of the 50 ks ACIS-S3 observation of 2000 January and 50 ks HRC-S observation of 2000 October have been reported by Murray et al. (2002). They found a low-significance period of 12 ms in the HRC-S data, which was not confirmed in the HRC-S observation of 2001 September (Ransom 2002), and concluded that the spectrum was consistent with that reported by Pavlov et al. (2000) and Chakrabarty et al. (2001). Hwang et al. (2004) presented beautiful images and spectra of the Cas A SNR obtained in the 1 Ms observations, but, regarding the CCO, they only mentioned that the best single-component model is a BB with $kT = 422 \pm 6$ eV and $R = (0.83 \pm 0.03)D_{3.4}$ km; that fit, however, was formally unacceptable ($\chi^2_\nu = 1.57$ for 315 degrees of freedom [dof]). The analysis of the ACIS observations of 1999–2004 did not show statistically significant changes of the CCO flux (Teter et al. 2004), virtually ruling out the possibility that the CCO emission is due to accretion. The spectral analysis of those data has shown that the fits with one-component thermal models (BB or NS atmosphere) leave large residuals at high energies, $E \gtrsim 4$ keV, suggesting that either the surface temperature is nonuniform or the emission at higher energies is of a nonthermal (e.g., magnetospheric) origin.

However, the spectral fits of those data, and the source properties inferred from those fits, suffered from large systematic uncertainties because all the “bare-ACIS” (no-grating) observations were taken in *full frame mode* (frame time 3.24 s), which resulted in a significant photon pileup¹, with $\sim 20\%$ pileup fraction for plausible spectral models. Although such a pileup fraction may look moderate, it substantially distorts the spectrum. In particular, it leads to an artificial excess of counts at higher energies (because two photons arriving within a frame are counted as one photon of higher energy), which can be easily confused with, e.g., a PL tail expected for active pulsars and magnetars.

Additional systematic errors in the bare-ACIS data of 1999–2004 were caused by the choice of Graded telemetry format² (to avoid telemetry saturation from the very bright SNR), which made it impossible to correct the spectra for Charge Transfer Inefficiency (CTI), and an off-axis placement of CCO (to image the SNR around the chip center), which blurred the CCO image and hampered the search for a possible pulsar wind nebula). Finally, in all but one of the 1 Ms observations the CCO was placed at the boundary between two CCD nodes, where “bad pixels” contaminate the data.

In the ACIS/HETG observation of the CCO, which did not suffer from pileup and was telemetered in Faint mode, the dispersed CCO spectrum was very strongly contaminated by the bright SNR background, while the zeroth order image had too few counts and was contaminated by the dispersed SNR image. In addition, there were virtually no source counts above 4 keV, where the ACIS/HETG effective area is very small.

The CCO was also observed with the EPIC

instrument onboard the *XMM-Newton* observatory (Mereghetti et al. 2002). However, because of the relatively low angular resolution, the CCO data were strongly contaminated by bright SNR filaments in the CCO vicinity.

Thus, despite the very deep observations taken, systematic errors, particularly those caused by pileup, have precluded an accurate spectral analysis of the CCO, crucial for understanding its nature. Therefore, we carried out another *Chandra* ACIS observation of the CCO, using a subarray of the only activated ACIS-S3 chip. The much shorter frame time of 0.34 s in this configuration allowed us to obtain a CCO spectrum virtually undistorted by pileup, and to search for pulsations with a period $\gtrsim 0.68$ s. Placing the target very close to the optical axis, we were able to image the immediate vicinity of the CCO with a high spatial resolution and search for compact extended emission (e.g., a pulsar wind nebula) that might be associated with the CCO.

In this paper we present the results of this observation. The data reduction is described in §2. In §3 we present the observational results, including the image analysis (§3.1), spectral analysis (§3.2), and timing (§3.3). Implications of the results and the possible nature of the CCO are discussed in §4.

2. OBSERVATIONS AND DATA REDUCTION

We observed the Cas A CCO on 2006 October 19 (ObsID 6690) with the *Chandra* ACIS detector for 70.181 ks in Timed Exposure mode, using Faint telemetry format. The target was imaged on the ACIS-S3 chip close to the optical axis (with a standard 20'' Y-offset to move the target from the node boundary). To minimize the photon pileup and improve time resolution, we used a 100 pixel subarray ($8.3' \times 0.82'$ field of view [FOV]) near the chip readout and turned off the other ACIS chips. In this observational setup, the frame time is 0.34104 s, which consists of 0.3 s exposure time and readout (dead) time of 41.04 ms required to transfer charge from the image region to the frame store region. Therefore, the effective target exposure time was 61.735 ks. There were no periods of substantially enhanced background during the observation.

We reduced the data using *Chandra* Interactive Analysis of Observations (CIAO) software³, ver. 4.1.2 (CALDB ver. 4.1.2). For the timing analysis, we transformed the event times of arrival to the solar system barycenter using the `barycen` tool. In our image analysis we used MARX⁴ and *Chandra* Ray Tracer (ChaRT) software⁵. We used XSPEC (ver. 12.0.4) for the spectral analysis.

3. DATA ANALYSIS AND RESULTS

3.1. Image

The $51'' \times 39''$ image of the CCO field is shown in Figure 1. The CCO looks like a pointlike source embedded in the SNR background. Using the CIAO `wavdetect` tool, we found the centroid of the CCO image at the coordinates

³ See <http://cxc.harvard.edu/ciao/>

⁴ MARX (Model of AXAF Response to X-rays) is a suite of programs designed to enable the user to simulate the on-orbit performance of the *Chandra* satellite. See <http://space.mit.edu/ASC/MARX/>

⁵ The software is available at <http://cxc.harvard.edu/chart/>.

¹ If two or more photons interact with the same detection cell within the frame time, they are registered as a single event. This effect is known as pileup (see §6.15 of The *Chandra* Proposers' Observatory Guide [POG], ver. 11, at <http://asc.harvard.edu/proposer/POG> for a detailed description).

² See §6.4.12 in POG.

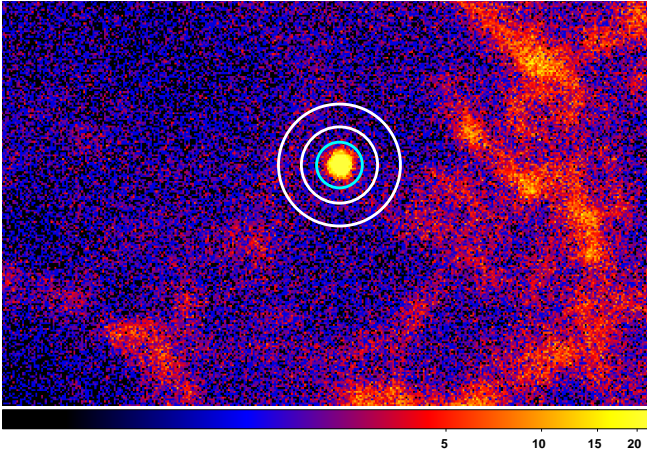


FIG. 1.— *Chandra* ACIS image, $51'' \times 39''$, of the Cas A CCO and its surroundings in the 0.6–6 keV band, after applying the subpixel event repositioning tool by Mori et al. (2001). The pixel size is $0.123''$ (i.e., $1/4$ of the original ACIS pixel size). The inner circle around the CCO shows the source extraction region of $1.476''$ radius used for the spectral analysis, while the annulus between $2.46''$ and $3.94''$ (white circles) is the background extraction region. The CCO is surrounded by non-uniform SNR emission, with the average surface brightness of 89 counts arcsec^{-2} in the $2.46''$ – $3.94''$ annulus.

$\alpha = 23^{\text{h}}23^{\text{m}}27.952^{\text{s}}$ and $\delta = +58^{\circ}48'42.57''$ (J2000). The CIAO `celldetect` tool yielded $\alpha = 23^{\text{h}}23^{\text{m}}27.956^{\text{s}}$ and $\delta = +58^{\circ}48'42.58''$. The differences of $0.03''$ and $0.01''$ in right ascension and declination, respectively, exceed the formal centroiding uncertainties (e.g., $0.006''$ per coordinate for the `wavdetect` measurement). They, however, are much smaller than the uncertainty of the *Chandra* absolute astrometry, $\approx 0.2''$ for each of the coordinates at the confidence level of 68% (Pavlov et al. 2009a), as estimated from the empirical distribution of radial offsets of X-ray positions with respect to the accurately known celestial locations for a sample of point sources⁶. The measured CCO coordinates are consistent with the most accurate of the previously measured coordinates (Fesen et al. 2006), within the uncertainties.

To look for an extended component in the CCO image, such as a pulsar wind nebula (PWN), and to choose an optimal extraction aperture for the spectral and timing analysis, we simulated a point source observation using ChaRT and MARX and compared the results with the observed count distribution. To reach a subpixel spatial resolution, we applied the subpixel event repositioning method (Mori et al. 2001) to both the observed and simulated images. For the simulation, we chose the spectral model $wabs \times nsa$ with the best-fit parameters (see §3.2 and Table 1) and simulated an ACIS-S3 observation for the same position on the detector and the same exposure time, 61.735 ks, as those of the actual observation. The width of the simulated point spread function (PSF) depends on the value of the MARX parameter `DitherBlur`. This parameter accounts for the ACIS pixelization and aspect reconstruction errors, which may be different for different observations. We simulated the PSF for a number of `DitherBlur` values, from $0.20''$ to $0.40''$, and found that the best match of the simulated PSF to the core of the observed image is provided by `DitherBlur` $\simeq 0.30''$. Figure 2 shows the simulated PSF radial profile and the

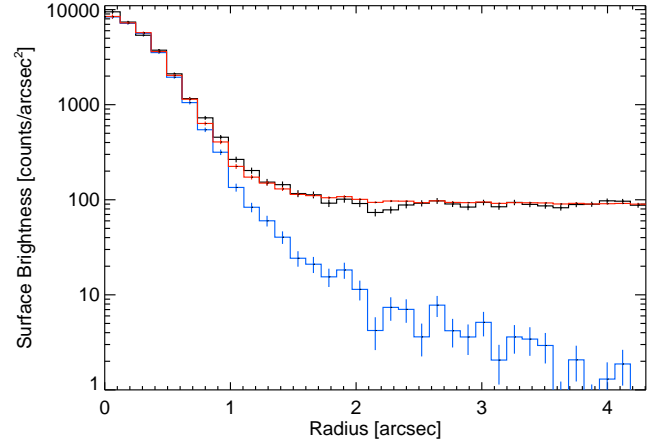


FIG. 2.— Radial profiles of the observed data (black) and the MARX-simulated PSF (blue) in the 0.6–6 keV band. The surface brightness was measured in the images with pixel size of $0.0615''$ ($1/8$ of the original ACIS pixel) in 35 circular annuli with $0.123''$ widths. The simulated PSF profile is for the MARX `DitherBlur` parameter of $0.30''$. The red histogram shows the sum of the simulated PSF and the model constant background, 89.6 counts arcsec^{-2} .

radial distribution of the detected events up to $4.3''$ from the source centroid. To calculate and plot these profiles, we rebinned the observed and simulated images to $1/8$ of the original ACIS pixel and measured the numbers of counts in circular annuli with widths of $0.123''$ ($1/4$ of the original pixel size). We see from this figure that the observed radial profile exceeds the simulated PSF at $r \gtrsim 1''$, remaining approximately constant at $r \gtrsim 2''$, with the average surface brightness of 89.6 ± 1.5 counts arcsec^{-2} in the $2'' < r < 4''$ annulus. The morphology of this extended emission on larger scales (see Fig. 1) suggests that it originates from the Cas A SNR (possibly belongs to a faint SNR filament), i.e., the extended emission is not a nebula generated by the CCO. This conclusion is supported by the presence of emission lines in the spectrum of this extended emission (see §3.2), which are not expected in the synchrotron spectrum of a PWN.

The sum of the simulated PSF and the uniform surface brightness of 89.6 counts arcsec^{-2} , shown by the red histogram in Fig. 2, is generally very close to the observed radial profile within the $r < 4.3''$ circle. It lies slightly below the observed data (i.e., the observed profile is slightly broader than the simulated one) at $0.7'' \lesssim r \lesssim 1.2''$, but the statistical significance of this difference is marginal (e.g., the largest discrepancy, in the 7th annulus, is significant at the 2σ level). The difference might be caused by a nonuniformity of the extended emission component at such radii or a minor inaccuracy of the MARX simulation, but it is hard to believe that the data excess is due to a PWN-like emission in this narrow region. An additional support for the pointlike structure of the CCO image is provided by the image deconvolution with the aid of the `arestore` script in CIAO (based on the Lucy-Richardson algorithm), performed by Kargaltsev et al. (2009) for the comparison with PSR J1617–5055 that is embedded in a PWN. These authors conclude that the deconvolved image of the Cas A CCO “preserves the pointlike appearance with no extended structure” (see Fig. 4 of that paper). Thus, we conclude that our ob-

⁶ See §5.4 and Fig. 5.4 in POG.

servation does not provide any substantial evidence for a PWN around the Cas A CCO.

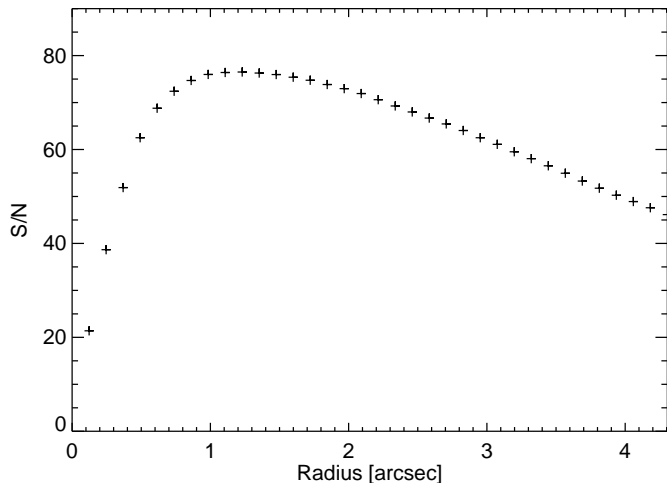


FIG. 3.— Signal-to-noise ratio as a function of circular aperture radius.

3.2. Spectral analysis

As the CCO is embedded in the significant SNR background, the source extraction region should be smaller than that for an isolated point source. To find an optimal extraction radius, we modeled the dependence of the signal-to-noise ratio (S/N) on the radius r of the source extraction aperture in the 0.6–6 keV band (Figure 3), using the above-described MARX simulation and the measured background surface brightness in the CCO vicinity. The S/N shows a flat maximum in the range $1.0'' \lesssim r \lesssim 1.5''$, with the peak value $S/N = 76.5$ at $r = 1.23''$. To minimize the spectral distortion caused by the increase of the PSF size with growing energy (i.e., the spectrum extracted from the PSF core is somewhat softer than the true spectrum), we chose the source aperture radius of $1.476''$ (three ACIS pixels), near the larger radius of the flat maximum. The MARX simulation shows that this circle contains 95.4% of total point source counts and 94.8% of total energy flux. Because the SNR background is not uniform (see Fig. 1), we have to choose the background extraction region sufficiently close to the CCO but not too close, in order to prevent the background “contamination” by the wings of the CCO’s PSF. After several trials, we chose the $2.46'' < r < 3.94''$ (5–8 ACIS pixels) annulus as the background region⁷.

⁷ To examine the effect of the source and background aperture sizes on the results of spectral fitting, we also fit the spectra extracted from the source apertures of $1.0''$ and $2.0''$ radii, and used

We used the CIAO `psextract` script to extract the spectra. The $1.476''$ radius aperture contains 7016 counts in the 0.6–6.0 keV range, of which about 607 counts belong to the background. This corresponds to the source count rate of 0.104 ± 0.02 counts s^{-1} in the source extraction region (or 0.109 ± 0.02 counts s^{-1} after correcting for the finite size of the extraction aperture). The source count rate of $\simeq 0.033$ counts per frame corresponds to the pile-up fraction (i.e., the ratio of the number of frames with two or more events to the number of frames with one or more events) of about 1.6%, a factor of 10–15 lower than in the previous ACIS observations with the frame time of 3.24 s.

We grouped the extracted spectrum with a minimum of 30 counts per spectral bin and fit it with several spectral models. The results are shown in Figures 4 and 5, and Table 1. The fit with the absorbed power-law (PL) model yields the photon index $\Gamma \approx 5$, much larger than $\Gamma = 1$ –2 for the X-ray spectra of active pulsars, and larger than $\Gamma = 3$ –4 obtained from the previous observations in which the CCO spectrum was considerably piled up. The observed flux, $F \approx 6.7 \times 10^{-13}$ erg cm^{-2} s^{-1} in the 0.6–6 keV band (7.0×10^{-13} erg cm^{-2} s^{-1} after correcting for the encircled energy fraction), is slightly lower than that found in the previous observations. The fit is marginally acceptable in terms of minimum χ^2 ($\chi^2_\nu = 1.21$ for $\nu = 125$ dof), but it shows excess data counts at lower energies ($\lesssim 1.2$ keV) and a deficit of data counts at higher energies ($\gtrsim 4.5$ keV). This suggests that the true spectral shape is different from the PL. In addition, the PL fit gives a rather large value for the hydrogen column density, $N_{H,22} \approx 2.8$, which not only strongly exceeds the total Galactic HI column density in that direction ($N_{HI,22} = 0.4$ –0.7; see Dickey & Lockman 1990; Kalberla et al. 2005) but is also substantially greater than typical values $N_{H,22} \approx 1.2$ –1.3 ($N_{H,22} = 1.5$ for a maximum value) in the CCO vicinity found from the fits of the SNR spectra with the absorbed two-component plasma emission model in the 1 Ms exposure data (Yang et al. 2008).

The fact that the observed spectrum is softer at higher energies than the best-fit PL model (even with the large Γ) suggests that a thermal model could provide a better description. The fit with the absorbed blackbody (BB) model gives⁸ temperatures $kT^\infty = 0.39$ –0.41 keV, hydrogen column densities $N_{H,22} = 1.2$ –1.4, radii of equivalent emitting sphere $R^\infty \approx (0.8$ –1.0) $D_{3.4}$ km ($R^\infty/D \approx 0.27$ km/kpc), and bolometric luminosities $L_{bol}^\infty \sim 3 \times 10^{33}$ erg s^{-1} . The temperatures are lower, and the radii are larger than those obtained from the piled-up spectra from the previous observations. The quality of the BB fit is considerably lower than that of the PL fit. Not only the BB fit gives a larger χ^2_ν (1.54 vs. 1.21), but it shows a

a few other annular background extraction regions. The spectral parameters obtained from those fits are generally consistent with those reported below (the differences are within the 2σ uncertainties).

⁸ We add the superscript ∞ to the temperature and radius to show that these parameter are quoted as observed by a distant observer, without any corrections for the gravitational effects. The temperature, radius and bolometric luminosity “at infinity” are connected with those as observed at the NS surface as follows: $T^\infty = Tg_r$, $R^\infty = R/g_r$, and $L_{bol}^\infty = L_{bol}g_r^2$, where $g_r = (1 - 2GM/Rc^2)^{1/2}$ is the gravitational redshift parameter.

strong excess of data counts at $E \gtrsim 4$ keV. Therefore, we conclude that the BB model gives a poorer description of the CCO spectrum than the PL model.

As the observed spectrum is harder than a BB but softer than a PL at higher energies, similar to the spectra of hydrogen (or helium) NS atmosphere (NSA)⁹ models (Pavlov et al. 1995; Zavlin et al. 1996), we fit it with a number of such models. An example of such a fit, for a hydrogen atmosphere model with a relatively low magnetic field ($B < 10^{10}$ G) and NS mass $M = 1.4M_{\odot}$ and radius $R = 10$ km ($g_r = 0.766$), is shown in Figure 4. In terms of χ^2_{ν} , the NSA fits are considerably better than the BB fit. Most of the NSA fits show an excess of data counts at high energies (e.g., 18.3 ± 7.7 counts in the 4.5–6 keV for the *wabs*×*nsa* fit shown in Figure 4), but it is not so strong as in the BB fits. Such an excess might be caused by the (small) pileup effect (which hardens the count spectrum, as mentioned in §1), but our estimates show that only a few such events are expected in our observation. The NSA models with high magnetic fields ($B >$ a few 10^{12} G) give worse fits than the low-field NSA models (in particular, a stronger excess at higher energies) because the spectra of high-field NSA models are closer to BB spectra (Pavlov et al. 1995). In comparison with the BB model, the low-field NSA models give a factor of 2 lower effective temperatures, $kT_{\text{eff}}^{\infty} = 0.17\text{--}0.20$ keV, and a factor of ~ 7 larger radius-to-distance ratio, $R^{\infty}/D = 1.3\text{--}1.7$ km/kpc, for $M = 1.4M_{\odot}$ and $R = 10$ km. For this mass and radius, the best-fit distances, $D = 7.5\text{--}10.1$ kpc, substantially exceed the measured distance to Cas A, suggesting a smaller size of the emitting region¹⁰, $R^{\infty} \sim 4\text{--}6$ km, considerably larger than for the BB fit but still too small for a NS radius [and comparable to the Schwarzschild radius, $R_s = 2.953(M/M_{\odot})$ km]. This suggests that either only a fraction of the NS surface is heated up to X-ray temperatures (in which case we should expect pulsations in the X-ray emission) or the CCO is not a NS at all (e.g., a strange quark star [SQS], whose radius can be considerably smaller than that of a NS). To explore the latter possibility, we fit the CCO spectrum with the *nsagrav* models, which allow one to vary M and R . An example of such a fit, in which the mass was fixed at $M = 0.25M_{\odot}$, the distance fixed at $D = 3.4$ kpc, and the radius was varied, is presented in Figure 4, for the best-fit parameters $R = 5.077$ km, $T_{\text{eff}} = 198$ eV, and $N_{\text{H},22} = 1.57$. The fit residuals are virtually indiscernible from those of the *nsa* fit (including the slight data excess at higher energies), and the T_{eff}^{∞} (but not T_{eff}) and $N_{\text{H},22}$ values are also almost the same. The corresponding bolometric luminosity is $L_{\text{bol}}^{\infty} \approx 4.2 \times 10^{33}$ erg s⁻¹, of which 91% is emitted in the 0.6–6 keV band. This fit confirms that the observed CCO emission might be interpreted as radiation emergent from a light-element atmosphere of an

object more compact than a NS. We will discuss such interpretations in more detail in §4.

If the CCO has a strong magnetic field and its magnetosphere contains a large number of energetic electrons, these electrons can Comptonize the NS thermal emission and generate a high-energy tail in the CCO spectrum. This effect can be crudely accounted for by the “resonance Compton scattering” (RCS) XSPEC model (Lyutikov & Gavriil 2006; Rea et al. 2008). The fit of the CCO spectrum with the RCS model is statistically good ($\chi^2_{\nu} = 1.11$), but it yields very broad ranges for the temperature of the seed BB emission, $kT \approx 0.1\text{--}0.2$ keV, and the normalization, $\approx 3 \times 10^{-5}\text{--}10^{-2}$, which are strongly anti-correlated (i.e., lower temperatures correspond to larger normalization parameters). The fit gives the resonant scattering optical depth $\tau_{\text{res}} = 1$ (at the lower boundary of the interval $\tau_{\text{res}} = 1\text{--}10$ included in the XSPEC set of the RCS models), and the characteristic velocity (in units of c) of the magnetospheric electrons $\beta_T = 0.24\text{--}0.35$. We see that the seed BB temperature is considerably lower than that found from the BB fit, which hints that the size of the emitting region is larger than BB radius, but, unfortunately, it remains unclear how the size could be estimated from the model normalization (N. Rea, priv. comm.). We should note, however, that, since the RCS model itself is substantially oversimplified (e.g., it assumes a one-dimensional motion of non-relativistic electrons with a rectangular velocity distribution along the radial direction), the inferred fitting parameters may be quite different from the actual physical parameters. Moreover, there is no even circumstantial evidence that the Cas A CCO has a magnetosphere densely populated by energetic particles (such as the non-thermal X-ray spectra in rotation-powered pulsars or the hard tails seen in magnetars even in quiescence). Therefore, the good fit may simply mean that the RCS model just mimics the observed CCO spectrum whose true origin may be quite different.

The quality of the spectral fits can be improved if we use various two-component models. Examples of such fits are shown in Figure 5 and Table 1. For instance, the PL+BB model (which is commonly used for the description of the X-ray spectra of rotation-powered pulsars, AXPs and SGRs) provides a good fit ($\chi^2_{\nu} = 1.12$; no excesses or deficits at lower and higher ends of the spectrum), but the slope of the PL component is still very steep ($\Gamma \approx 4.6$), the size of the BB-emitting region is still much smaller than the NS radius (≈ 1.2 km at $D = 3.4$ kpc), and the hydrogen column density is too large ($N_{\text{H},22} \approx 2.3$).

The BB+BB model (which can be considered as a crude model for thermal emission from the surface with a non-uniform temperature) gives a good fit ($\chi^2_{\nu} = 1.11$), with $kT_{\text{soft}}^{\infty} \approx 0.3$ keV, $R_{\text{soft}}^{\infty} \approx 2$ km, $L_{\text{bol,soft}}^{\infty} \approx 4.1 \times 10^{33}$ erg s⁻¹ for the low-temperature (soft) component, and $kT_{\text{hard}}^{\infty} \approx 0.6$ keV, $R_{\text{hard}}^{\infty} \approx 0.25$ km, $L_{\text{bol,hard}}^{\infty} \approx 0.6 \times 10^{33}$ erg s⁻¹ for the high-temperature (hard) component (the radii and luminosities are for $D = 3.4$ kpc). Although the addition of another BB component has resulted in a larger size, this size is still much smaller than the NS radius.

Obviously, one could obtain a larger emitting size using a two-component NSA model. The NSA+NSA fit with

⁹ The hydrogen NSA models are dubbed *nsa* and *nsagrav* in XSPEC. The *nsa* models are for fixed NS mass and radius, $M = 1.4M_{\odot}$ and $R = 10$ km ($R^{\infty} = 13.06$ km, gravitational acceleration at the NS surface $g = 2.43 \times 10^{14}$ cm s⁻²); in these models the distance is the fitting parameter. The *nsagrav* models include a set of NSA models on a mass-radius grid; therefore, they allow one to fit the mass and radius for a given distance.

¹⁰ Although the spectral shape depends on the assumed M and R , in contrast with the BB spectrum, the dependence is weak, so that the radius can be rescaled as $R \propto D$ for crude estimates.

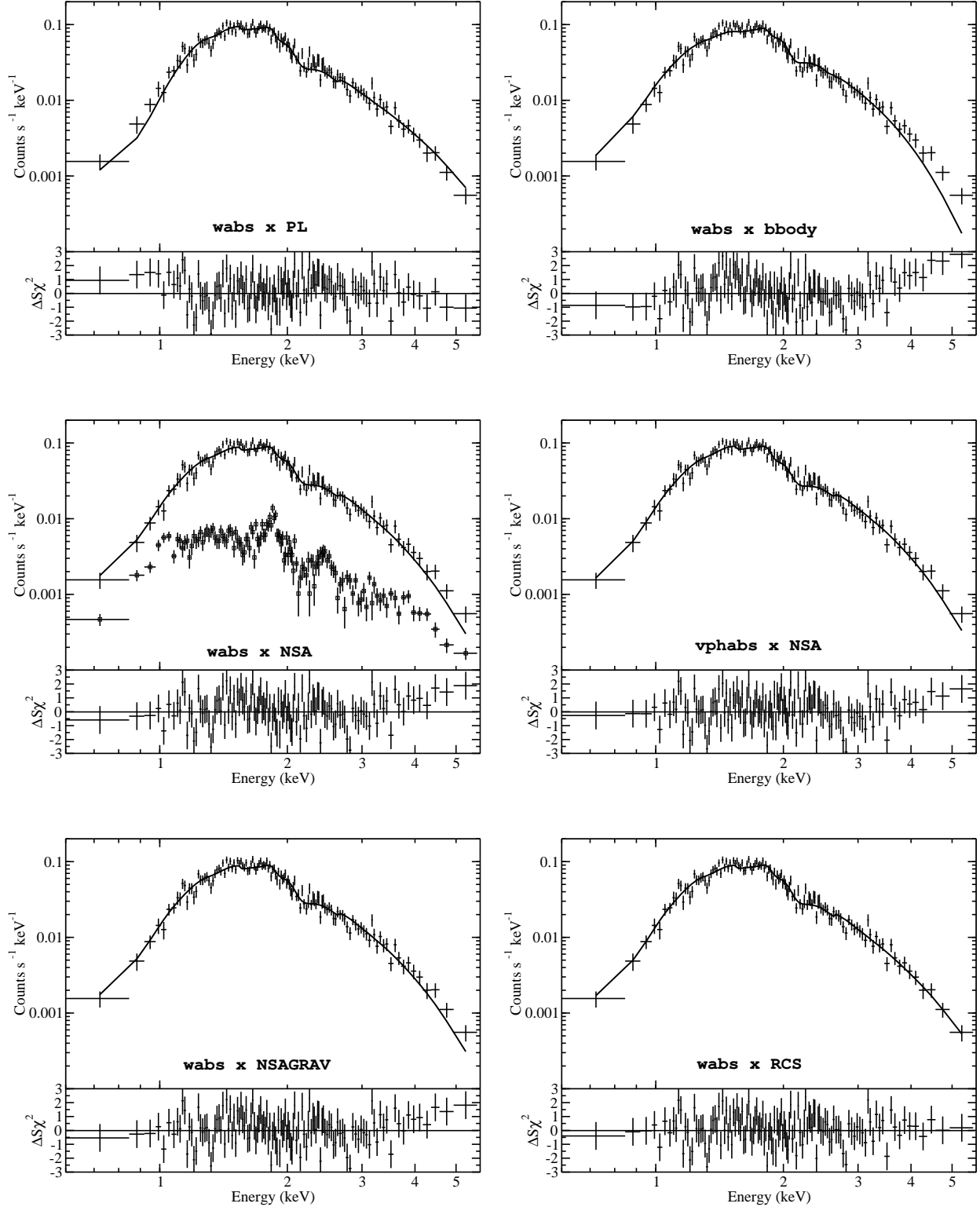


FIG. 4.— Fits of the CCO spectrum extracted from the $1.476''$ aperture with absorbed one-component spectral models (see Table 1 for the fitting parameters). The *wabs*×*NSA* panel also shows the background contribution.

low-field *nsa* models gives the temperatures $T_{\text{eff,soft}}^{\infty} \approx 0.14$ keV and $T_{\text{eff,hard}}^{\infty} \approx 0.4$ keV. The range of distances for the soft component, $D = 1.8\text{--}5.9$ kpc, includes the

range of 3.3–3.7 kpc inferred by Reed et al. (1995) for the Cas A SNR. Moreover, if we rescale $R_{\text{soft}}^{\infty} = 13.06$ km to $R_{\text{soft}}^{\infty} \approx 11$ km, still consistent with a NS radius,

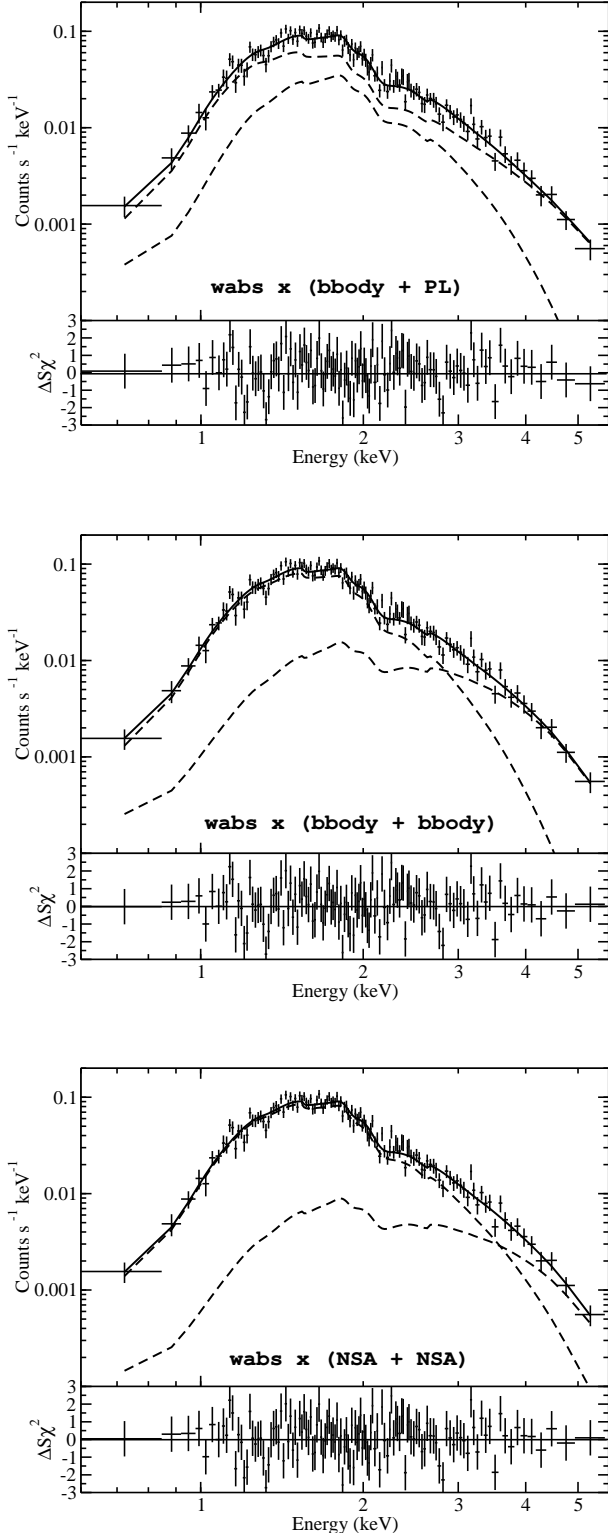


FIG. 5.— Fits of the CCO spectrum extracted from the 1.476'' aperture with absorbed two-component models (see Table 1 for the fitting parameters). The component contributions are shown by dashed lines.

it would correspond to the best-fit distance of 3.4 kpc, equal to the most probable distance to Cas A. The similarly scaled size for the hard component is ~ 0.4 km, for $D = 3.4$ kpc. For these effective temperatures and scaled radii, the bolometric luminosities are $L_{\text{bol,soft}}^{\infty} \approx 5.7 \times 10^{33}$ erg s $^{-1}$ and $L_{\text{bol,hard}}^{\infty} \approx 0.4 \times 10^{33}$ erg s $^{-1}$. Thus, we cannot rule out that the CCO is a NS with a nonuniform surface temperature, although it is hard to explain the nonuniformity without assuming a strong magnetic field of a special topology (see §4).

In all the fits described above, we see some structure in the residuals, in the range of ≈ 1 –3 keV, which hints at the presence of spectral lines or photoabsorption edges. If real, such spectral features could be either intrinsic features in the CCO spectrum (e.g., similar to the absorption lines detected in the spectrum of the CCO 1E1207.4–5209; Sanwal et al. 2002) or they might be caused by photoabsorption between the source and the observer if the element abundances are different from those adopted in the *wabs* photoabsorption model used in the above fits. To explore the latter possibility, we applied the *vphabs* photoabsorption model with variable abundances together with the NSA model. Fitting the abundances of the elements with photoionization edges in the 0.6–3 keV range (Fe, Ne, Mg, Si, S), we found that the Fe, Ne, S and Mg abundances were poorly constrained and consistent with the solar values, while the Si abundance showed some excess¹¹. Fixing the abundances of all the elements but Si at their solar values, we obtained the Si abundance of 3.2 ± 1.3 , without substantial changes of the other fitting parameters (see Table 1). The fit shows a marginal improvement with respect to the *wabs* \times *nsa* fit ($\chi^2_{\nu} = 1.19$ vs. 1.24) and somewhat smoother residuals in the 1.5–2.5 keV range, but it does not affect the structure at 1.1–1.4 keV and the apparent absorption feature around 2.8 keV.

We have checked that such features could not be caused by inaccurate subtraction of the SNR background, which does not show spectral lines at these energies (see the panel *wabs* \times *nsa* in Figure 4). However, our simulations of ACIS count rate spectra for continuum spectral models show that similar “features” often appear because of statistical fluctuations. We also examined the spectra obtained in the previous, much longer observations of the CCO and found no features at these energies for most of them¹². Therefore, we conclude that, most likely, our observation does not show real spectral features in the CCO spectrum.

3.3. Timing

To search for the CCO period, we used the arrival times for the 6756 events extracted from the 1.23'' radius aperture (which provides maximum S/N ; see Figure 3) in the 0.6–6.0 keV band (the estimated background contribution is 421 events). With the frame time $t_{\text{frame}} = 0.34104$ s, we can search for periods $P > 2t_{\text{frame}} = 0.68208$ s (frequencies $f < 1.466$ Hz). We calculated the Z_1^2 (Rayleigh)

¹¹ Possible additional absorption at the Si-K photoionization edge, 1.84 keV, has been noticed by Stage et al. (2004) in previously observed spectra of the CCO. These authors interpret it as caused by material in the Cas A SNR.

¹² We should mention, however, that the stronger parallel CTI effect in those observations might wash out faint spectral features.

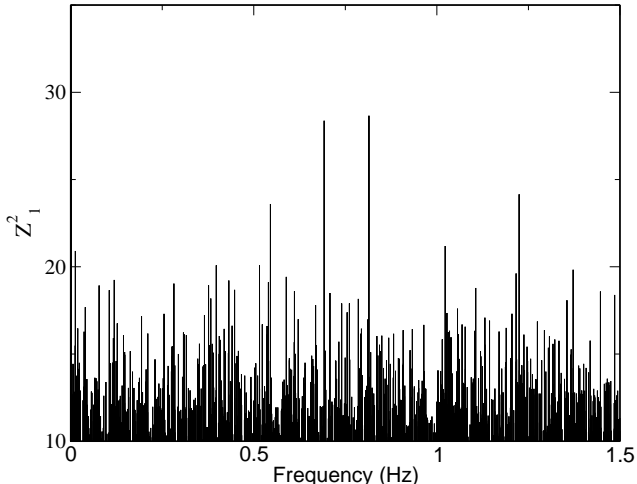


FIG. 6.— Power spectrum $Z_1^2(f)$ for the Cas A CCO.

statistic (Buccheri et al. 1983) as a function of frequency (i.e., the power spectrum) in the range $30 \mu\text{Hz} < f < 1.466 \text{ Hz}$ with the step $\Delta f = 1 \mu\text{Hz} \approx 0.07 T_{\text{span}}^{-1}$, where $T_{\text{span}} = 70, 181 \text{ s}$ is the time span of our observation. The power spectrum is shown in Figure 6. The highest peaks in the power spectrum, $Z_1^2 = 28.66$ and 28.38 , are found at the frequencies $f = 0.814487$ and 0.692145 Hz , respectively (the frequency uncertainty is about $2 \mu\text{Hz}$ for each of the peaks). If, for instance, the highest peak were due to the actual pulsations, it would correspond to the pulsed fraction $p = p_{\text{obs}}(N_S + N_B)N_S^{-1} \approx [2Z_1^2(N_S + N_B)]^{1/2}N_S^{-1} \pm [2(N_S + N_B)]^{1/2}N_S^{-1} = 0.098 \pm 0.018$ (for a nearly sinusoidal signal), where $N_S = 6333$ and $N_B = 421$ are the numbers of source and background counts in the source aperture, and p_{obs} is the pulsed fraction uncorrected for the background contribution. However, the probability of obtaining such a peak by chance in a noise spectrum is $f_{\text{max}}T_{\text{span}} \exp(-Z_1^2/2) = 0.061$, which corresponds to the confidence level of only 1.87σ . Given the low confidence level and the presence of a few other peaks of similar heights (see Figure 6), we have to conclude that this observation does not show pulsations with a period $P \gtrsim 0.68 \text{ s}$. Following the approach by Groth (1975), the upper limits on the pulsed fraction p can be estimated as 13%, 14% or 16% at the confidence levels of 95%, 99% or 99.9%, respectively.

From their analysis of the *XMM-Newton* observation of the Cas A CCO, Mereghetti et al. (2002) report somewhat lower values of the pulsed fraction upper limits (e.g., $p < 13\%$ in the 0.4–2 Hz band at the 3σ level). That observation, however, suffered from the strong, nonuniform SNR background, whose contribution into the source aperture could hardly be measured with a sufficient accuracy. Indeed, the fact that the CCO’s flux reported by Mereghetti et al. is a factor of 3 higher than the value we measured with *Chandra* (see Table 1) suggests that the background contribution, $N_B/(N_S + N_B)$, is 92% rather than 75% estimated in that paper, and the background-corrected upper limit on the pulsed fraction is also a factor of 3 higher than reported by Mereghetti et al.

4. DISCUSSION

Our observation of the Cas A CCO with the *Chandra* ACIS detector in subarray mode has allowed us to obtain the most accurate X-ray spectrum, virtually undistorted by pileup, to look for extended emission in the high resolution image of this source, and to search for periodicity with periods greater than 0.68 s. The results of this observation can be used not only to measure the source properties with high precision, but also to put new constraints on its nature.

The very high X-ray-to-optical flux ratio (e.g., $F_X/F_H > 10^4$; Fesen et al. 2006) proves unequivocally that the Cas A CCO is indeed a compact object associated with the Cas A SNR, not a usual star or a background AGN. It is generally believed that a compact source born in a Type II SN explosion can be either a NS or a black hole. If the Cas A CCO were a black hole, its X-ray emission could be only due to accretion of the ambient matter, in which case we would expect a substantial variability (as accretion is an inherently unstable process) and strong emission lines generated in the hot accreting matter. However, the CCO’s flux has not shown stastically significant changes in numerous *Chandra* observations (Teter et al. 2004), its X-ray spectrum does not show strong emission lines (§3.2), and its X-ray luminosity is too high to be explained by accretion of SNR material onto the apparently fast-moving CCO (Pavlov et al. 2000). Therefore, we conclude that the black hole interpretation can be ruled out.

Most of the known NSs are rotation-powered pulsars (~ 1800 such pulsars have been detected in the radio, ~ 80 in X-rays, ~ 30 in γ -rays, and ~ 10 in the optical). X-ray observations of rotation-powered pulsars usually show hard PL components in their spectra (with photon index $\Gamma \sim 1-2$), interpreted as magnetospheric emission, with sharp pulsations. Moreover, virtually all young, powerful pulsars are accompanied by bright PWNe generated by the winds of ultrarelativistic particles ejected from the pulsar magnetosphere (e.g., Kargaltsev & Pavlov 2008). As the X-ray spectrum of the radio- and γ -ray-quiet CCO is very soft (almost certainly thermal; see §3.2), and, more importantly, there are no traces of a PWN around the CCO (§3.1), we have to conclude that it is not a rotation-powered pulsar.

The usual (rotation-powered) pulsar activity could be quenched in a young NS if its rotation is too slow or its magnetic field is too weak to generate strong electric fields at and above the NS surface, needed for normal pulsar operation. Very high magnetic fields (\gtrsim a few 10^{13} G) can also inhibit the pulsar activity (perhaps, by suppressing electron-positron pair production because of photon splitting in a superstrong magnetic field; Baring & Harding 1998), as we know from observations of magnetars. Thus, the Cas A CCO could belong to one of the two known types of young NSs without pulsar activity — magnetars, which are characterized by superstrong magnetic fields ($B \sim 10^{14}-10^{15} \text{ G}$) and slow rotation ($P = 2-12 \text{ s}$), and “anti-magnetars” (Gotthelf & Halpern 2008), which are NSs with low magnetic fields ($B \lesssim 10^{11} \text{ G}$) and moderately fast rotation, whose periods ($P \sim$ a few 0.1 s) have changed very little during their lifetime. Also, we cannot exclude the opportunity that the CCO represents a new type of a compact object, perhaps with an exotic composition, such as a

strange quark star (SQS; Witten 1984). We will discuss these options below, with account for our observational results.

4.1. A magnetar?

A strong support for the magnetar interpretation could be provided by detection of pulsations with a period of a few seconds, typical for magnetars. We found no evidence for pulsations, with an upper limit on pulsed fraction of about 10%–15%, for $P > 0.68$ s. The non-detection, however, does not prove that the CCO is not a magnetar because some of them have an even lower pulsed fraction (Woods & Thompson 2006).

The shape of the CCO’s X-ray spectrum resembles those of magnetars in the *Chandra* energy band. For instance, the PL+BB model satisfactorily describes the spectra of both the CCO and magnetars. However, according to Table 4.1 in Woods & Thompson (2006), the magnetar BB temperatures (0.4–0.7 keV) inferred from such fits are somewhat higher than the temperature of the BB component in the CCO’s spectrum, 0.30–0.38 keV, while the magnetar photon indices ($\Gamma = 2$ –4) are somewhat smaller than the photon index of the CCO’s PL component, $\Gamma = 3.6$ –5.2. The fitting parameters obtained from the RCS fits are also close to those obtained by Rea et al. (2008) for some AXPs. However, the CCO’s X-ray luminosity, $L_X \sim 4 \times 10^{33}$ erg s $^{-1}$, is lower than those of magnetars, $L_X \sim 10^{34}$ – 10^{35} erg s $^{-1}$. It would be very interesting to compare the spectra of the CCO and magnetars at $E > 10$ keV, where magnetars show very hard PL spectra ($\Gamma = 1$ –1.5 for the total [pulsed + nonpulsed] emission), but it would require hard X-ray instruments with high spatial resolution to separate the CCO’s emission from the much brighter Cas A SNR’s emission.

If the CCO were a magnetar, we would expect bursts and flares. However, we have not seen any significant flux variations in the 10 years of *Chandra* observations. In fact, if in the last ~ 40 years the CCO had produced a flare on a scale we see in SGRs, it would likely have been detected by an all-sky monitor in hard X-rays or soft γ -rays. There was a claim by Krause et al. (2005) that the apparent motions of Cas A filaments with tangential velocities close to the speed of light, observed with *Spitzer* at 24 μ m, could be interpreted as an infrared echo of a strong flare from the CCO ~ 60 years ago, but this interpretation has been retracted by Kim et al. (2008) and Dwek & Arendt (2008).

One might speculate that the CCO does possess a superstrong magnetic field, perhaps hidden in the NS interior, but, being so young, it has not yet developed the properties we see in “mature” magnetars. Such an interpretation is in line with the hypothesis by Bhattacharya & Soni (2007), who suggest that the superstrong magnetic field in a very young magnetar is originally concentrated in the NS core, and it will require $\gtrsim 10^3$ yr for this field to reach the crust and give rise to the magnetar activity. It is hardly possible to confirm or reject this interpretation of the CCO by direct observations (unless a burst or a flare is detected). In the framework of this hypothesis, the X-ray emission from the CCO should be thermal, with luminosity and temperature perhaps somewhat higher than those of “usual” NSs due to additional heat that might be released in

the NS interiors by dissipation of the “hidden” superstrong magnetic field, and its spectrum should be best described by an NSA model. The observed spectrum generally does not contradict this hypothesis, at least if we believe that the NS surface temperature is nonuniform, but this would not be a unique interpretation. The interpretation will perhaps look more plausible if the scenario by Bhattacharya & Soni (2007) is supported by detailed studies of established magnetars (i.e., AXPs and SGRs). To conclude, the magnetar interpretation of the Cas A CCO does not seem very likely, but it cannot be ruled out, especially the assumption that the CCO is an “immature” magnetar.

4.2. An anti-magnetar?

In addition to the Cas A, CCOs in several other SNRs are known, with similar properties (Pavlov et al. 2002, 2004; de Luca 2008). Those CCOs also show thermal-like X-ray spectra, albeit with temperatures and luminosities lower than those of the Cas A CCO, and they also do not show pulsar or magnetar activity. It seems natural to explore the possibility that the nature of the Cas A CCO is the same as of the other CCOs, just the Cas A CCO is younger.

Unlike the Cas A CCO, pulsations have been discovered in three CCOs, with periods in the range of 0.105–0.424 s (Zavlin et al. 2000; Gotthelf et al. 2005; Gotthelf & Halpern 2009). Surprisingly, the upper limits on period derivatives turned out to be very low (Gotthelf & Halpern 2007, 2009; Halpern et al. 2007), corresponding to spin-down luminosities, $\dot{E} \equiv 4\pi^2 I \dot{P} P^{-3}$, lower than the X-ray luminosities (which means that the X-ray emission is not powered by NS rotation). To explain the fact that the corresponding lower limits on spin-down ages are much larger than the SNR ages, $\tau_{\text{sd}} \equiv P/2\dot{P} \gg T_{\text{SNR}}$, one has to assume that the initial spin periods of these pulsars were very close to their current values, $P_0 = P(1 - T_{\text{SNR}}/\tau_{\text{sd}})^{1/2}$. As the upper limits on the magnetic fields¹³, $B \equiv 3.2 \times 10^{19} (P\dot{P})^{1/2} \lesssim$ a few $\times 10^{11}$ G, turned out to be much lower than those of magnetars (and even of young rotation-powered pulsars), these objects were dubbed “anti-magnetars” by Gotthelf & Halpern (2008), who also suggested that the Cas A CCO may be a member of this class of NSs.

The current data, including our new observation, do not contradict the assumption that the Cas A CCO is indeed an anti-magnetar. The non-detection of period is not conclusive because the shortest period we would be able to detect is longer than the periods of the known anti-magnetars, and the upper limit on pulsed fraction is not low enough to exclude weak pulsation even at these long periods (e.g., the pulsed fractions of the CCOs in the PKS 1209–51/52 and Puppis A SNRs are about 9% and 11%, respectively). The Cas A CCO spectrum is

¹³ For the best-investigated CCO, 1E1207.4–5209 in the PKS 1209–51/52 SNR, the magnetic field, $B_{\text{cycl}} = 6 \times 10^{10} g_r^{-1}$ G was estimated from the absorption features (Sanwal et al. 2002) interpreted as harmonics of the electron cyclotron frequency (Bignami et al. 2003). A very close value of the magnetic field, $B_{\text{sd}} = 9.7 \times 10^{10}$ G, has been recently estimated from the period derivative determined with the aid of new *XMM-Newton* observations (Pavlov et al. 2009b).

well described by the same spectral models as those of anti-magnetars, with similar spectral parameters. Similar to the anti-magnetars, the spectra are thermal (or at least they contain a strong thermal component), but a single-component BB model does not give good fits. A single-component NSA model gives acceptable fits, but the radii of equivalent emitting sphere are smaller than a reasonable NS radius. Two-component models, such as BB+BB, give very good fits, but the NS surface layers at so high temperatures and low magnetic fields are expected to be gaseous (plasma) atmospheres, whose spectra are different from BB because photons with different energies emerge from layers with different temperatures. Therefore, a more realistic description of the thermal emission from anti-magnetars should be based on NSA models rather than the BB model.

As the magnetic field of an anti-magnetar is low, and the spin period is relatively long, accretion of SN debris soon after the SN explosion is possible. If there is even a very small fraction of hydrogen or helium in the accreted material, the emission emerges from a hydrogen or helium NS atmosphere because of the gravitational stratification. If the field is much lower than 10^{11} G, it makes no effect on the NSA X-ray emission, so that the use of low-field NSA models is justified. If the field is around 10^{11} G (as in 1E1207–5209), cyclotron absorption features are expected in the *Chandra* energy band. This would require the use of NSA models with the cyclotron energy in the soft X-ray range (currently unavailable in XSPEC), but the continua of such models are rather close to the low-field NS spectra (Suleimanov et al. 2009). The relatively low fit quality and too small size of the emitting region in the single-component NSA fit suggests that the NS surface temperature is not uniform. As we do not know the temperature distribution over the surface, we have to use the simplest approximation of two regions with different temperatures and areas (e.g., a hot spot and a colder bulk surface). Our fit with the NSA+NSA model has given a very good fit, with temperatures $T_{\text{eff,soft}}^{\infty} \approx 1.6$ MK, $T_{\text{eff,hard}}^{\infty} \approx 4.6$ MK, and radii $R_{\text{soft}}^{\infty} \approx 11$ km and $R_{\text{hard}} \sim 0.4$ km, for $D = 3.4$ kpc. The bolometric luminosities of the two components are $L_{\text{soft}}^{\infty} \approx 5.7 \times 10^{33}$ erg s $^{-1}$ and $L_{\text{hard}}^{\infty} \sim 0.4 \times 10^{33}$ erg s $^{-1}$, assuming isotropic emission. Since the bolometric luminosity and the temperature of the soft component are consistent with the predictions of various NS cooling models (e.g., Tsuruta 1998) for the Cas A CCO age, the soft component can be interpreted as emission of the thermal energy stored in the NS interiors. However, it is not easy to explain the origin of a small hot spot at the NS surface. At such low magnetic fields, the anisotropy of thermal conductivity, which may lead to a nonuniform temperature distribution (e.g., the magnetic poles are hotter than the equator because the conductivity is higher along the magnetic field), is negligible, and, moreover, this effect could not produce such a small hot spot even in a superstrong magnetic field for the dipole geometry (Pérez-Azorín et al. 2006). Pavlov et al. (2000) speculated that the temperature anisotropy could be due to a nonuniform chemical composition over the NS surface (e.g., there might be hydrogen “islands”, perhaps formed by accretion onto the magnetic poles soon after the SN explosion, on the iron surface that is colder

than the islands because the thermal conductivity of the degenerate NS envelope is proportional to the inverse nucleus charge, Z^{-1}). However, this interpretation looks somewhat artificial, and it has not been supported by observational data (e.g., heavy-element spectral lines in the CCO spectrum). Alternatively, the hot spot(s) could be heated by ongoing slow accretion from a residual debris disk onto the magnetic pole(s), but there are no observational indications, such as flux variability or emission spectral lines, of such accretion. Another way to explain the origin of small hot spot(s) is to assume the presence of a very strong toroidal magnetic field, $B \gtrsim 10^{13}$ G, in the NS crust (Pérez-Azorín et al. 2006). Such a field could screen the heat flux from the NS interior toward the surface in a broad range of magnetic latitudes around the equator, leading to a large temperature contrast between the poles and the rest of the NS surface (see Figs. 8 and 9 in Pérez-Azorín et al. 2006). Although the toroidal field would not penetrate into the NS surface layers and would not affect the NS spin-down (which is determined by a much lower poloidal [e.g., dipole] component in this model), the hypothesis about the presence of a very strong toroidal component in anti-magnetars may look somewhat artificial. In a sense, within the framework of this hypothesis, anti-magnetars become similar to the “immature magnetars” in the scenario by Bhattacharya & Soni (2007).

To conclude, the interpretation of the Cas A CCO as a young anti-magnetar seems very plausible, but there is no unequivocal explanation for the nonuniformity of the surface temperature. This problem, however, is pertinent to the established anti-magnetars, too. The anti-magnetar interpretation of the Cas A CCO could be confirmed by a measurement of the CCO period with a small period derivative, which would require dedicated observations¹⁴ with a timing resolution considerably better than 0.1 s. A firm proof of a low surface magnetic field could be provided by detection of two or more spectral features associated with cyclotron harmonics, which would require deep observations with an observational setup similar to that used in our observation. To resolve the problem of nonuniform temperature of anti-magnetars and understand the temperature and field distributions over the NS surface, phase-resolved spectroscopy, interpreted with the aid of NSA models with appropriate magnetic fields, would be most helpful.

4.3. A strange quark star?

As we have seen in §3.2, reasonably good fits to the Cas A CCO spectrum are provided by the NSA models with a uniform effective temperature, but these fits imply a small emitting area, much smaller than the visible area of a NS. To infer the allowed range of masses and radii of the CCO, assuming that it is covered by a low-field hydrogen atmosphere, we have fit the observed spectrum with the *nsagraw* models on a grid in the R - M plane. Each of such fits yields the distance to the source, through the model normalization. This allows one to plot the lines of constant distance (and strips corresponding to ranges

¹⁴ A 300 ks observation with the *Chandra* HRC-S detector, aimed at the search for the CCO period, has been carried out recently (2009 March; PI D. Chakrabarty), but no results have been published yet.

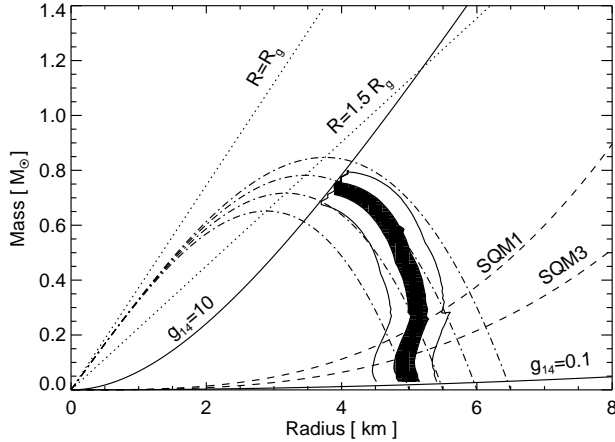


FIG. 7.— Mass-radius region compatible with the distance to the CCO, obtained from the *wabs* × *nsaggrav* fits. The black strip corresponds to $D = 3.3\text{--}3.5$ kpc, while the white strips leftward and rightward of the black strip correspond to $D = 3.1\text{--}3.3$ and $3.5\text{--}3.7$ kpc, respectively. The dotted lines correspond to $R = R_g$ and $R = 1.5R_g$, where R_g is the gravitational (Schwarzschild) radius; the solid lines, $g_{14} \equiv g/10^{14} \text{ cm s}^{-2} = 10$ and 0.1 , correspond to the maximum and minimum gravitational accelerations for which the *nsaggrav* models are available. The $M(R)$ curves for two models of strange quark matter equation of state, SQM1 and SQM3, are shown by dashed curves. The dash-dotted curves are the loci of constant R^∞ (note that $R^\infty \rightarrow R$ for $M \rightarrow 0$).

of distances) in the R - M plane. Figure 7 shows such strips around the line corresponding to $D = 3.4$ kpc, the most probable distance to Cas A (Reed et al. 1995); the black strip ($D = 3.3\text{--}3.5$ kpc) is enveloped by the strips for $D = 3.1\text{--}3.3$ and $3.5\text{--}3.7$ kpc. We see that the maximum allowed radius R of the compact object is about 5.5 km, while the apparent radius $R^\infty < 6.5$ km, and the object’s mass cannot exceed $0.8M_\odot$. This R - M domain is inconsistent with any NS equation of state, but it is consistent with low-mass SQS models. The $M(R)$ curves for two equations of state of strange quark matter, SQM1 and SQM3 (Lattimer & Prakash 2001), shown in Figure 7, cross the R - M domain allowed by the *nsaggrav* fits at $R \approx 4.5\text{--}5.5$ km; they correspond to the allowed mass ranges $M \approx 0.2\text{--}0.3$ and $0.1\text{--}0.2 M_\odot$, respectively. The effective temperature and bolometric luminosity, $T_{\text{eff}}^\infty \approx 2.1$ MK and $L_{\text{bol}}^\infty \approx 4 \times 10^{33} \text{ erg s}^{-1}$, do not change significantly within the strips.

Thus, the emission from the CCO could, in principle, be interpreted as emerging from a SQS atmosphere which could form above a normal-matter crust (Glendenning & Weber 1992). The main problem with this interpretation is the very low star’s mass. For instance, if the SQS is formed as a result of a phase transition in a NS, we would not expect the SQS mass to be lower than $\approx 1M_\odot$. One might speculate that the SQS was formed directly in the SN explosion, but we are not aware of SN models that would result in such a low-mass compact remnant. On the other hand, we cannot be sure that such a scenario is impossible. Therefore, we believe that the SQS interpretation, however exotic it looks, should not be dismissed until rejected by further observations. A possible way to check it would be very deep observations in the near-IR (more suitable than the optical because of the high extinction), which could detect the Rayleigh-Jeans tail of thermal emission from

the bulk of the NS surface. If the small region associated with the CCO X-ray emission is, in fact, just a heated area on the NS surface, while the rest of the surface is substantially colder, the near-IR observation could detect this colder emission and prove that its size is much larger than that seen in X-rays. The current deepest near-IR limit, inferred from *HST* NICMOS observations, is $H > 24.6$ (Fesen et al. 2006), but the emission from the NS surface is expected to be even fainter, i.e., deeper observations are required to detect it. The SQS interpretation would also be called into question if future X-ray observations show this object to be an anti-magnetar. (Although anti-magnetars might, in principle, be SQSs, the more conventional NS interpretation is preferable until proven otherwise, according to the Occam’s razor.)

4.4. Summary

To summarize, we believe that the anti-magnetar interpretation of the Cas A CCO, similar to the three other CCOs proven to be anti-magnetars, is currently the most plausible. In this interpretation, the CCO’s emission with the bolometric luminosity $L_{\text{bol}}^\infty \sim 6 \times 10^{33} \text{ erg s}^{-1}$ emerges from a NS atmosphere with nonuniform effective temperature, relatively low magnetic field, $B \lesssim 10^{11}$ G, and very slow spin-down. The origin of the temperature nonuniformity is not clear, as well as for the other anti-magnetars; it might be caused by a much stronger toroidal magnetic field in the NS crust. The most direct way to check the anti-magnetar interpretation is to measure the CCO’s period and period derivative and/or detect spectral features that could be interpreted as harmonics of the electron cyclotron frequency.

There is no observational evidence of the Cas A CCO being a magnetar similar to the currently known SGRs and AXPs. We, however, cannot rule out the possibility that it is an immature magnetar, whose ultrastrong magnetic field is hidden in the NS interiors and does not make a strong effect on the observable properties. If this is the case, the Cas A CCO may eventually turn into an “ordinary” magnetar, but we consider this hypothesis rather speculative.

Finally, we cannot firmly reject the possibility that the Cas A CCO is a SQS, with a radius of ≈ 5 km and a mass $\lesssim 0.8M_\odot$, covered by a normal-matter crust and an atmosphere with $kT_{\text{eff}}^\infty \approx 0.18$ keV and $L_{\text{bol}}^\infty \approx 4 \times 10^{33} \text{ erg s}^{-1}$. It remains unclear how the SQS with so low mass could be formed. Future observations will help check this interpretation.

We thank Slava Zavlin for calculating *nsaggrav* models for a broader parameter domain, Dany Page for providing the NS and SQS $M(R)$ relations for various equations of state, Leisa Townsley for the discussions of the CTI effects in ACIS, Nanda Rea for the discussion of the RCS spectral model, Sandro Mereghetti for the discussion of the *XMM-Newton* observation of Cas A, and Oleg Kargaltsev, Zdenka Misanovic and Bill Joye for their useful advice on the data analysis. Support for this work was provided by the National Aeronautics and Space Administration through *Chandra* Award Number GO6-7055X issued by the *Chandra* X-ray Observatory Center, which is operated by the Smithsonian Astrophysical Observatory for and on behalf of the National Aeronau-

tics Space Administration under contract NAS8-03060. NNX09AC84G.
The work was also partially supported by NASA grant

REFERENCES

- Aschenbach, B. 1999, IAU Circ. 7249
 Aschworth, W. B. 1980, *J. Hist. Astron.*, 11, 1
 Baring, M. G., & Harding, A. K. 1998, *ApJ*, 507, L55
 Bhattacharya, D., & Soni, V. 2007, preprint arXiv:0705.0592v1
 Bignami, G. F., Caraveo, P. A., de Luca, A., & Mereghetti, S. 2003, *Nature*, 423, 725
 Bucccheri, R., et al., 1983, *A&A*, 128, 245
 Chakrabarty, D., Pivovarov, M. J., Hernquist, L. E., Heyl, J. S., & Narayan, R. 2001, *ApJ*, 548, 800
 de Luca, A. 2008, in 40 Years of Pulsars: Millisecond Pulsars, Magnetars and More, AIP Conf. Proc., 983, 311
 Dickey, J. M. & Lockman, F. J., 1990, *ARA&A*, 28, 215
 Dwek, E., & Arendt, R. G. 2008, *ApJ*, 685, 976
 Fesen, R. A., Pavlov, G. G., & Sanwal, D. 2006, *ApJ*, 636, 848
 Glendenning, N. K., & Weber, F. 1992, *ApJ*, 400, 647
 Gotthelf, E. V., Halpern, J. P., & Seward, F. D. 2005, *ApJ*, 627, 390
 Gotthelf, E. V., & Halpern, J. P. 2007, *ApJ*, 664, L35
 Gotthelf, E. V., & Halpern, J. P. 2008, in 40 Years of Pulsars: Millisecond Pulsars, Magnetars and More. AIP Conf. Proc., 983, 320
 Gotthelf, E. V., & Halpern, J. P. 2009, *ApJ*, 695, L35
 Groth, E. J. 1975, *ApJS*, 29, 285
 Hwang, U., et al. 2004, *ApJ*, 615, L117
 Halpern, J. P., Gotthelf, V. E., Camilo, F., & Seward, F. D. 2007, *ApJ*, 665, 1304
 Kalberla, P. M. W., Burton, W. B., Hartmann, Dap, Arnal, E. M. et al., 2005, *A&A*, 440, 775
 Kargaltsev, O., & Pavlov, G. G. 2008, in 40 Years of Pulsars: Millisecond Pulsars, Magnetars, and More, AIP Conf. Proc., 983, 171
 Kargaltsev, O., Pavlov, G. G., & Wong, J. A. 2009, *ApJ*, 690, 891
 Kim, Y., Rieke, G. H., Krause, O., Misselt, K., Indebetouw, R., & Johnson, K. E. 2008, *ApJ*, 678, 297
 Krause, O., et al. 2005, *Science*, 308, 1604
 Lattimer, J. M., & Prakash, M. 2001, *ApJ*, 550, 426
 Lyutikov, M., & Gavriil, F. P. 2006, *MNRAS*, 368, 690
 Mereghetti, S., Tiengo, A., & Israel, G.L. 2002, *ApJ*, 569, 275
 Mori, K., Tsunemi, H., Miyata, E., Baluta, C. J., Burrows, D. N., Garmire, G. P., & Chartas, G. 2001, in New Century of Astronomy, ASP Conf. Proc., v.251, ed. H. Inoue & H. Kunieda (San Francisco: ASP), 576
 Murray, S. S., Ransom, S. M., Juda, M., Hwang, U., & Holt, S. S. 2002, *ApJ*, 566, 1039
 Pavlov, G. G., Shibanov, Y. A., Zavlin, V. E., & Meyer, R. D., 1995, in *The Lives of the Neutron Stars*. eds. M. A. Alpar, U. Kiziloglu and J. van Paradijs (Kluwer: Dordrecht) p.71
 Pavlov, G. G., & Zavlin, V. E. 1999, IAU Circ. 7270
 Pavlov, G. G., Zavlin, V. E., Aschenbach, B., Trümper, J., & Sanwal, D. 2000, *ApJ*, 531, L53
 Pavlov, G. G., Sanwal, D., Garmire, G. P., & Zavlin, V. E. 2002, in *Neutron Stars in Supernova Remnants*, ASP Conf. Ser., v. 271, eds. P.O. Slane & B. Gaensler, p.247
 Pavlov, G. G., Sanwal D., & Teter M. A. 2004, in *Young Neutron Stars and Their Environments*, IAU Symp. 218, eds. F. Camilo and B. M. Gaensler (San Francisco, CA: ASP) p.239
 Pavlov, G. G., Kargaltsev, O., Wong, J. A., & Garmire, G. P. 2009a, *ApJ*, 691, 458
 Pavlov, G. G., Woods, P. M. & Zavlin, V. E. 2009b, *ApJ*, in preparation
 Pérez-Azorín, J. F., Miralles, J. A., & Pons, J. A. 2006, *A&A*, 451, 1009
 Ransom, S. M. 2002, in *Neutron Stars in Supernova Remnants*, ASP Conf. Ser., v.271, eds. P. O. Slane & B. M. Gaensler, p.361
 Rea, N., Zane, S., Turolla, R., Lyutikov, M., & Götz, D. 2008, *ApJ*, 686, 1245
 Reed J. E., Hester J. J., Fabian A. C. & Winkler P. F., 1995, *ApJ*, 440, 706
 Sanwal, D., Pavlov, G. G., Zavlin, V. E., & Teter, M. A. 2002, *ApJ*, 574, L61
 Stage, M. D., Joss, P. C., Madej, J., Rózińska, A. 2004, *Adv. Space Res.*, 33, 606
 Suleimanov, V., Pavlov, G. G., & Werner, K. 2009, *ApJ*, in preparation
 Tananbaum, H. 1999, IAU Circ. 7246
 Teter, M. A., Pavlov, G. G., Tsuruta, S., & Liebman, A. 2004, *AAS Meeting 204*, #74.13
 Tsuruta, S. 1998, *Phys. Rep.*, 292, 1
 Witten, E. 1984, *Phys. Rev. D* 30, 272
 Woods, P. M., & Thompson, C. J. 2006, in *Compact Stellar X-ray Sources*, ed. W. Lewin & M. van der Klis, Cambridge Astrophys. Ser. No. 39 (Cambridge, UK: Cambridge Univ. Press), 547
 Yang, X., Lu, F., Chen, Li, 2008, *ChJAA*, 8, 439
 Zavlin, V. E., Pavlov, G. G., Sanwal, D., & Trümper, J., 2000, *ApJ*, 540, L25
 Zavlin, V. E., Pavlov, G. G., & Shibanov, Yu. A. 1996, *A&A*, 315, 141

TABLE 1
FITTING PARAMETERS FOR DIFFERENT SPECTRAL MODELS

Model	$N_{\text{H},22}^{\text{a}}$	Γ^{b}	$kT^{\infty\text{c}}$	$\mathcal{N}_{-2}^{\text{d}}$	R^{∞}/D^{e}	F_{-13}^{f}	$F_{-12}^{\text{un,g}}$	χ^2_{ν} (dof)
<i>wabs</i> ×PL	$2.81^{+0.13}_{-0.13}$	$5.23^{+0.17}_{-0.16}$...	$1.38^{+0.29}_{-0.23}$...	$6.68^{+0.17}_{-0.17}$	$35.58^{+8.99}_{-6.85}$	1.21(125)
<i>wabs</i> ×BB	$1.32^{+0.08}_{-0.07}$...	402^{+11}_{-11}	...	$0.91^{+0.09}_{-0.07}/3.4$	$6.53^{+0.17}_{-0.17}$	$1.84^{+0.14}_{-0.12}$	1.54 (125)
<i>wabs</i> × <i>nsa</i> ^h	$1.57^{+0.08}_{-0.10}$...	185^{+9}_{-8}	...	$13.06/8.5^{+1.6}_{-1.0}$	$6.62^{+0.17}_{-0.17}$	$2.47^{+0.24}_{-0.20}$	1.24 (125)
<i>wabs</i> × <i>nsagrav</i> ⁱ	$1.57^{+0.09}_{-0.08}$...	182^{+8}_{-8}	...	$5.49^{+0.74}_{-0.64}/3.4$	$6.61^{+0.15}_{-0.14}$	$2.81^{+0.23}_{-0.32}$	1.25 (125)
<i>vphabs</i> × <i>nsa</i> ^j	$1.46^{+0.10}_{-0.08}$...	190^{+4}_{-13}	...	$13.06/8.5^{+1.1}_{-1.4}$	$6.62^{+0.17}_{-0.17}$	$2.82^{+0.26}_{-0.33}$	1.19/(124)
<i>wabs</i> ×RCS ^k	$1.64^{+0.07}_{-0.06}$...	283^{+25}_{-180}	$6.69^{+0.18}_{-0.17}$	$2.80^{+3.64}_{-0.24}$	1.11(124)
<i>wabs</i> ×(PL+BB)	$2.27^{+0.36}_{-0.49}$	$4.62^{+0.56}_{-1.07}$...	$0.44^{+0.55}_{-0.36}$	$6.70^{+0.17}_{-0.17}$	$9.96^{+8.34}_{-6.14}$	1.12 (123)
...	332^{+52}_{-30}	...	$1.19^{+0.46}_{-0.57}/3.4$...	$1.37^{+0.31}_{-0.25}$...
<i>wabs</i> ×(BB+BB)	$1.71^{+0.21}_{-0.17}$...	305^{+35}_{-38}	...	$1.92^{+0.97}_{-0.51}/3.4$	$6.68^{+0.17}_{-0.18}$	$2.45^{+0.49}_{-0.37}$	1.11(123)
...	614^{+170}_{-90}	...	$0.19^{+0.15}_{-0.11}/3.4$...	$0.45^{+0.18}_{-0.12}$...
<i>wabs</i> ×(<i>nsa</i> + <i>nsa</i>)	$1.81^{+0.81}_{-0.80}$...	141^{+27}_{-35}	...	$13.06/4.2^{+1.7}_{-2.4}$	$6.68^{+0.17}_{-0.17}$	$3.24^{+0.69}_{-0.53}$	1.11(123)
...	394^{+92}_{-86}	...	$13.06/119^{+180}_{-85}$...	$0.28^{+0.23}_{-0.12}$...

NOTE. — The fits are for the source spectrum extracted from the 1.476'' radius aperture, background taken from the 2.26''–3.94'' annulus. The errors of fitting parameters are given at the 90% confidence level for one interesting parameter.

^a Hydrogen column density in units of 10^{22} cm^{-2} .

^b Photon index for PL spectra.

^c Effective temperature as seen by a distant observer, in units of eV.

^d PL normalization = photon spectral flux at 1 keV, in units of $10^{-2} \text{ photons cm}^{-2} \text{ s}^{-1} \text{ keV}^{-1}$.

^e Radius (as seen by a distant observer) in units of km, and distance in kpc. In the *nsa* model, the NS radius and mass are fixed at $R = 10 \text{ km}$ and $M = 1.4M_{\odot}$ ($R^{\infty} = 13.06 \text{ km}$), while the distance is the fitting parameter.

^f Observed (absorbed) energy flux in the 0.6–6 keV band, in units of $10^{-13} \text{ ergs cm}^{-2} \text{ s}^{-1}$, calculated with the *cflux* model in XSPEC.

^g Unabsorbed energy flux in the 0.6–6 keV band, in units of $10^{-12} \text{ ergs cm}^{-2} \text{ s}^{-1}$, calculated with the *cflux* model in XSPEC. The corresponding luminosity is $L_X = 1.38 \times 10^{33} F_{-12}^{\text{un}} \text{ erg s}^{-1}$, for $D = 3.4 \text{ kpc}$.

^h NSA model for fixed $M = 1.4M_{\odot}$ and $R = 10 \text{ km}$.

ⁱ The fit is for fixed $M = 0.25M_{\odot}$. The distance (normalization) was fixed, while the radius R is a fitting parameter ($R = 5.08^{+0.68}_{-0.59} \text{ km}$).

^j The result is for variable Si abundance; its fitted value is $3.2^{+1.3}_{-1.3}$.

^k Fit with the resonance Compton scattering model, for fixed $\tau_{\text{res}} = 1.0$. In addition to N_{H} and kT , the fitting parameters are $\beta_T = 0.33^{+0.02}_{-0.09}$ and $\text{norm} = 0.7^{+100}_{-0.5} \times 10^{-4}$.